Supplemental Materials

A. Details of the finite field calculations

In finite field calculations, the polarizability is obtained as either the second derivative of the energy (energy-derivative method) or the first derivative of the dipole moment (dipole-derivative method). This section shows that the dipole derivative method is more stable with respect to the magnitude of the field used to calculate the finite-difference derivatives, and with respect to the number of orbitals included in the SCI calculation.

Figure S1 shows the polarizability of the $1B_u$ excited state and of the ground state along the long inertial axis of stilbene, α_{xx} ($1B_u$) and α_{xx} (gs), for various values of the finite field used to evaluate the energy and dipole derivatives. As discussed by Kurtz[1], accurate results are expected for an intermediate range of field strengths. For field magnitudes smaller than the optimal range, errors in the finite-difference derivative result from the change in energy or dipole being small compared to the numerical error in these calculated quantities. For field magnitudes greater than the optimal range, errors result from the contribution of higher-order derivatives to the finite-difference derivative. Figure S1 demonstrates that the dipole-derivative method is more robust than the energy-derivative method with regards to the finite field strength. The optimal range of the dipole-derivative method spans six orders of magnitude (5 $V \cdot cm^{-1}$ to 5×10^6 $V \cdot cm^{-1}$), while the optimal range of the energy-derivative method spans only three orders of magnitude (5×10^3 $V \cdot cm^{-1}$ to 5×10^6 $V \cdot cm^{-1}$). This is not surprising given that the energy-derivative method involves evaluation of second derivatives while the dipole-derivative method involves only first derivatives.

Figure S2 illustrates that the dipole-derivative method is also more robust with regards to truncation of the number of orbitals included in the SCI calculation. The polarizability calculated for the $1B_u$ excited state, $Tr\overleftrightarrow{\Delta\alpha}$, is shown for planar and linear oligomers with n=2, 4, and 8. The calculations include all π and π^* orbitals, and the number of σ and σ^* orbitals is increased from zero to full SCI. The polarizability obtained from the dipole derivative method shows a monotonic convergence with respect

to the number of sigma orbitals, while that obtained from the energy derivative method shows substantial oscillations. For each oligomer, there is a truncation of the orbital space that causes the energy-derivative method to give polarizabilities that differ substantially from the converged value.

B. Green's function in dielectric screening model

Figure S3 illustrates the Green's function $G\left(\left|\mathbf{r}_i - \mathbf{r}_j\right|\right)$ used in Eq. (5) to calculate the dielectric solvation energy of a charge distribution. As discussed in the main text, the short range form of $G\left(\left|\mathbf{r}_i - \mathbf{r}_j\right|\right)$ is obtained from explicit calculations for charges in a conjugated polymer environment (the solid line of Figure S3). Eq. (6) gives the long range behavior of $G\left(\left|\mathbf{r}_i - \mathbf{r}_j\right|\right)$ as a function of dielectric constant (the broken lines of Figure S3). The form used in this work is obtained by splicing the short-range behavior of $G\left(\left|\mathbf{r}_i - \mathbf{r}_j\right|\right)$, obtained from explicit calculations, with the long range behavior appropriate for a dielectric constant of 2.0.

C. Comparison of OPPV-9 and PPV-8

This section examines the effects of hydroxyl substitution on the excited state energies and polarizabilities in PPV type polymers. Figure S4 shows the excited state energies of the PPV-8 and OPPV-9 oligomers as a function of the strength of the dielectric screening. Figure 6 of the main text shows the relationship between $Tr\overleftrightarrow{\Delta\alpha}$, ΔE, and the strength of the dielectric screening for PPV-8. Figure S5 is an analogous figure for OPPV-9, and illustrates that the relationships between the quantities are essentially the same in PPV-8 as in OPPV-9. This validates the use of un-substituted PPV oligomers as models of substituted species, for the quantities considered in this work. It further demonstrates that the large polarizability of these polymers is not a consequence of the substituents on the phenylene rings, but is rather an intrinsic property of these conjugated systems.

Based on the linear fits for the polarizabilities of these two oligomers (shown as insets in Figures 6 and S5), when the $1B_u$-mA_g energy gap is between 0.55 and 0.65 eV,

$Tr\overleftrightarrow{\Delta\alpha}$ is estimated to be in the range of 2100-3000 Å^3 for PPV-8, and 2000-2900 Å^3 for OPPV-9.

E. Modeling outer-sphere disorder through explicit solvent molecules

An explicit environment of MeTHF solvent molecules was created using quenched molecular dynamics with the Universal Force Field[2] as implemented in Molecular Simulations Inc.'s Cerius[2] software package. Charges were obtained from AM1 calculations on an isolated PPV-8 oligomer and an isolated MeTHF molecule, and the charges were held fixed throughout the simulations. Starting with a large crystalline sample of MeTHF, the central MeTHF molecules were removed and the PPV-8 oligomer was placed in the resulting cavity. For all simulations and minimizations, the PPV-8 structure was fixed at the planar structure obtained from AM1 calculations. The sample was then truncated, retaining the 194 MeTHF molecules that were within 20 Å of the PPV oligomer. A molecular dynamics trajectory was run at 1000K (temperature scaling with a window of ±50K) using leap-frog integration and a time step of 2 fs. To obtain well randomized structures, Coulomb interactions were turned off during the molecular dynamics. Four structures were obtained at intervals of 6ps. Coulomb interactions were then turned back on and the energy of each of these four structures was minimized. Visual inspection revealed un-physically large density fluctuations (*i.e.* voids) in the resulting structures. This can attributed to these calculations being done on a gas-phase cluster, rather than at constant pressure. We are currently investigated improved means of using molecular mechanics to generate explicit glassy environments. For this work, we instead utilized the random dipole lattices described below to model the glassy environment.

D. Modeling outer-sphere disorder through the dipole lattice model

The main text presents results obtained using a lattice of randomly oriented dipoles to model the permanent charge distributions present in the amorphous solid-state environment. The dependence of the results on the lattice parameters is shown in Table S1. The distributions of $\Delta\mu_x$ and $Tr\overleftrightarrow{\Delta\alpha}$ converge rapidly with respect to the size of the lattice (the number of solvent shells included around the oligomer) when all other

parameters are fixed, as shown by lattices 1 through 9 in Table S1. This suggests that the first few shells of dipole moments dominate the interaction with the oligomer. Increasing the effective density of the dipoles by either increasing their magnitude (lattices 14-16) or decreasing the spacing between sites (lattices 13 and 14) broadens the distribution of both $Tr\overrightarrow{\Delta\alpha}$ and $\Delta\mu_x$, and shifts the peak of the distribution of $Tr\overrightarrow{\Delta\alpha}$ to larger values. The results are also sensitive to the size of the cavity (lattices 10-13), especially in the direction perpendicular to the plane of the PPV-8 oligomer. Increasing the distance from the plane containing the oligomer to the closest dipole from 3 to 6 Å lowers the rms-$\overrightarrow{\Delta\mu}$ by a factor of 2, from lattice 10 to lattice 13. Lattice 17 shows that the rms-$\overrightarrow{\Delta\mu}$ is quite small when dielectric screening of electron-hole interactions is ignored.

Reference List

1. Kurtz, H. A.; Stewart, J. J. P.; Dieter, K. M. *J. Computational Chem.* **1990**, *11*(1), 82-87.

2. Rappe A K; Casewit C J; Colwell K S; Goddard W A III; Skiff W M *J. Am. Chem. Soc.* **1992**, *114*(25), 10024-35.

Table S1. Summary of dipole lattice model calculations. All calculations are done at the INDO/SCI level, with inclusion of all excitations beween the π and π* orbitals.

Lattice type	Cavity size	Number of shells	Magnitude of the dipole (Debye)	ΔE (eV)	Δα (Å^3)	rms-Δμ (Debye)	Note
1	(7.5, 6.5, 6)	1	0.96	0.72 ± 0.05	1800 ± 300	5.9	
2		2		0.70 ± 0.08	2000 ± 400	7.9	
3		3		0.7 ± 0.1	2200 ± 800	10.4	
4		4		0.68 ± 0.09	2100 ± 600	9.4	
5		5		0.7 ± 0.1	2100 ± 600	11.3	
6		8		0.7 ± 0.1	2200 ± 800	9.8	
7		11		0.68 ± 0.09	2100 ± 1000	13.7	
8		14		0.70 ± 0.09	2000 ± 600	8.7	
9		20		0.7 ± 0.1	2100 ± 700	9.9	
10	(4.5, 3.5, 3)	5	0.96	0.6 ± 0.2	3000 ± 3000	21.5	
11	(7.5, 3.5, 3)			0.5 ± 0.2	4000 ± 3000	20.9	
12	(4.5, 6.5, 3)			0.6 ± 0.2	3000 ± 2000	21.1	
13	(4.5, 3.5, 6)			0.7 ± 0.1	2000 ± 1000	10.2	
14	(4.5, 3.5, 6)	5	0.96	0.75 ± 0.01	1600 ± 100	3.5	
15			1.92	0.70 ± 0.09	2000 ± 500	7.6	6[a]
16			2.72	0.6 ± 0.1	3000 ± 1000	13.5	
17	(7.5, 6.5, 6)	5	0.96	1.362 ± 0.009	420 ± 20	1.7	gas[b]

a) The lattice site spacing is 6 Å for lattices 14-16, while all other lattice types have site spacing of 3 Å.
b) The solvation scaling factor is zero for row 17, which is a gas phase calculation. All other lattice types have solvation scaling factor 1.0.

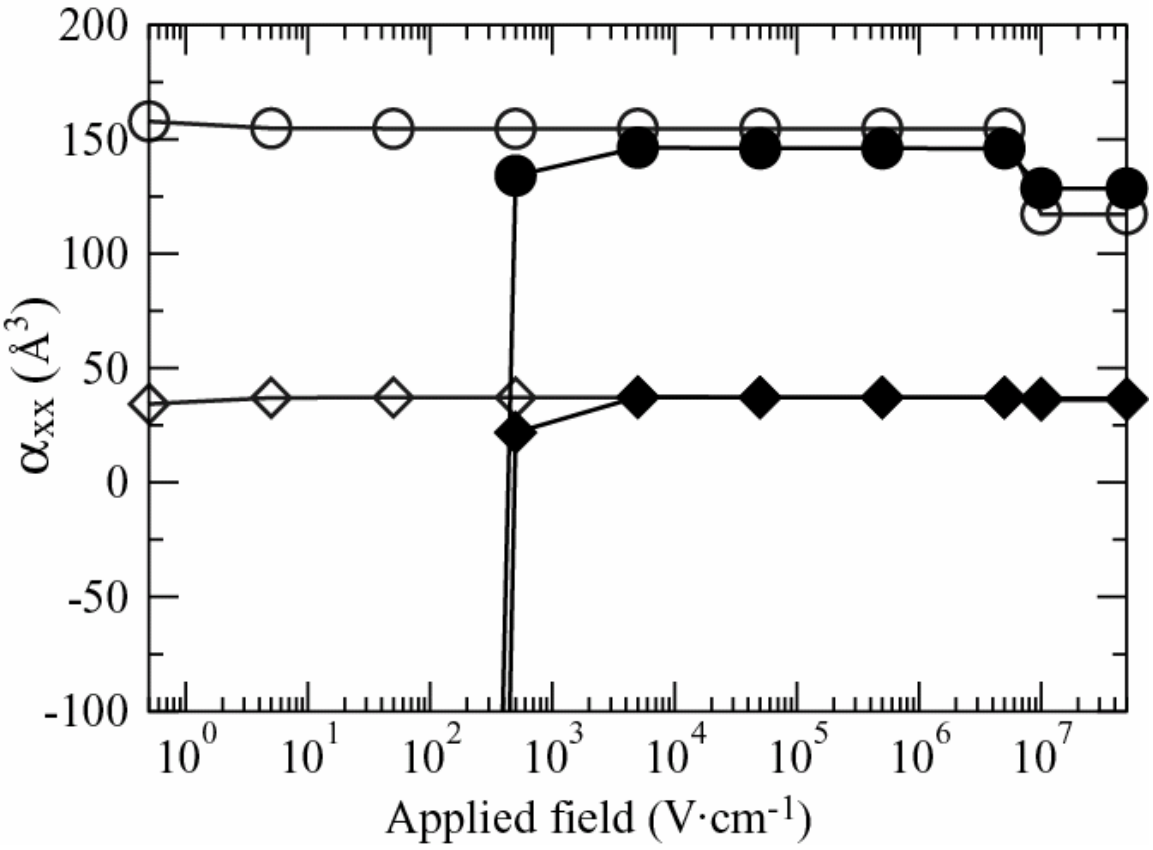

Fig. S1. Polarizability along the long inertial axis of stilbene, α_{xx} ($1B_u$) and α_{xx} (gs), obtained from the energy-derivative and dipole-derivative methods, as a function of the magnitude of the finite field used to evaluate the derivatives. The circles represent α_{xx} ($1B_u$) and the diamonds represent α_{xx} (gs); the filled symbols are from the energy-derivative calculations, and the empty symbols are from the dipole-derivative calculations.

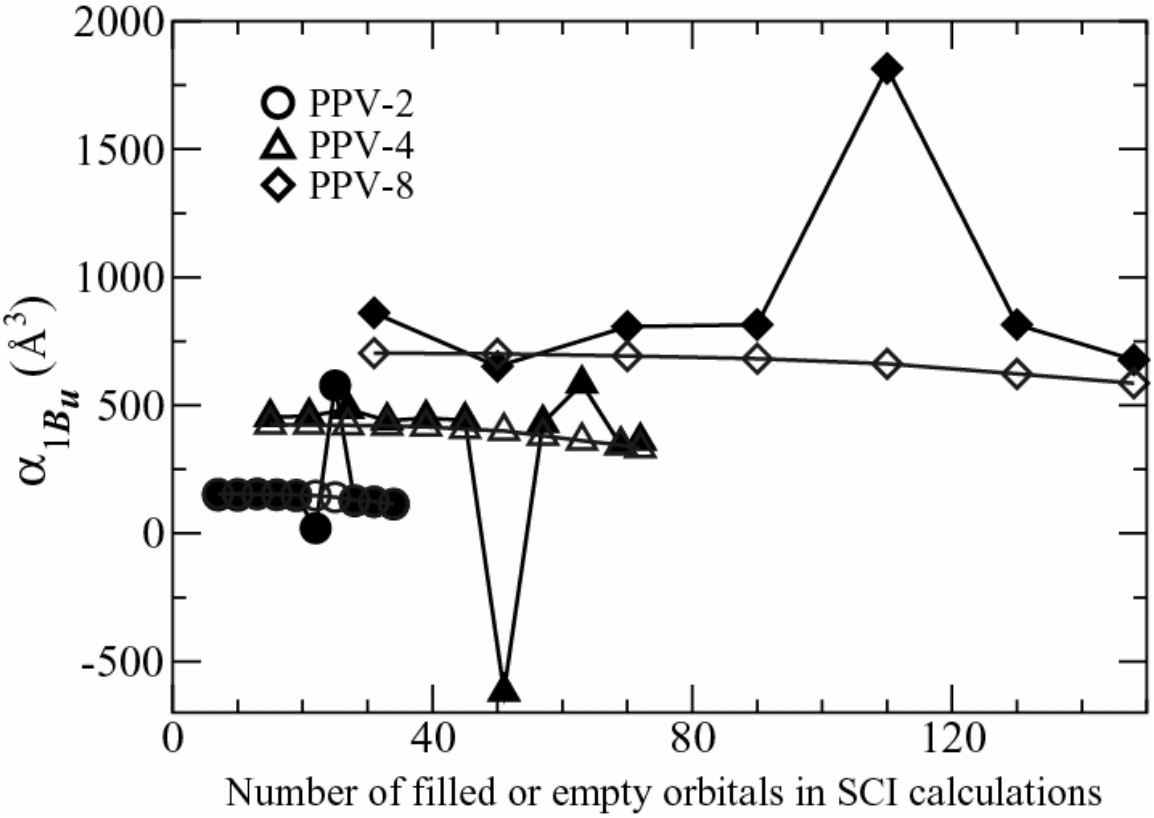

Fig. S2. $Tr\overleftrightarrow{\Delta\alpha}$ of the $1B_u$ excited state obtained from the energy-derivative and dipole-derivative methods, as a function of the number of orbitals included in the SCI calculation. Results are shown for three planar PPV oligomers with n=2 (circles), n=4 (triangles) and n=8 (diamonds). The filled symbols are from the energy-derivative calculations, and the empty symbols are from the dipole-derivative calculations. The calculations are done for an isolated oligomer, without inclusion of dielectric screening.

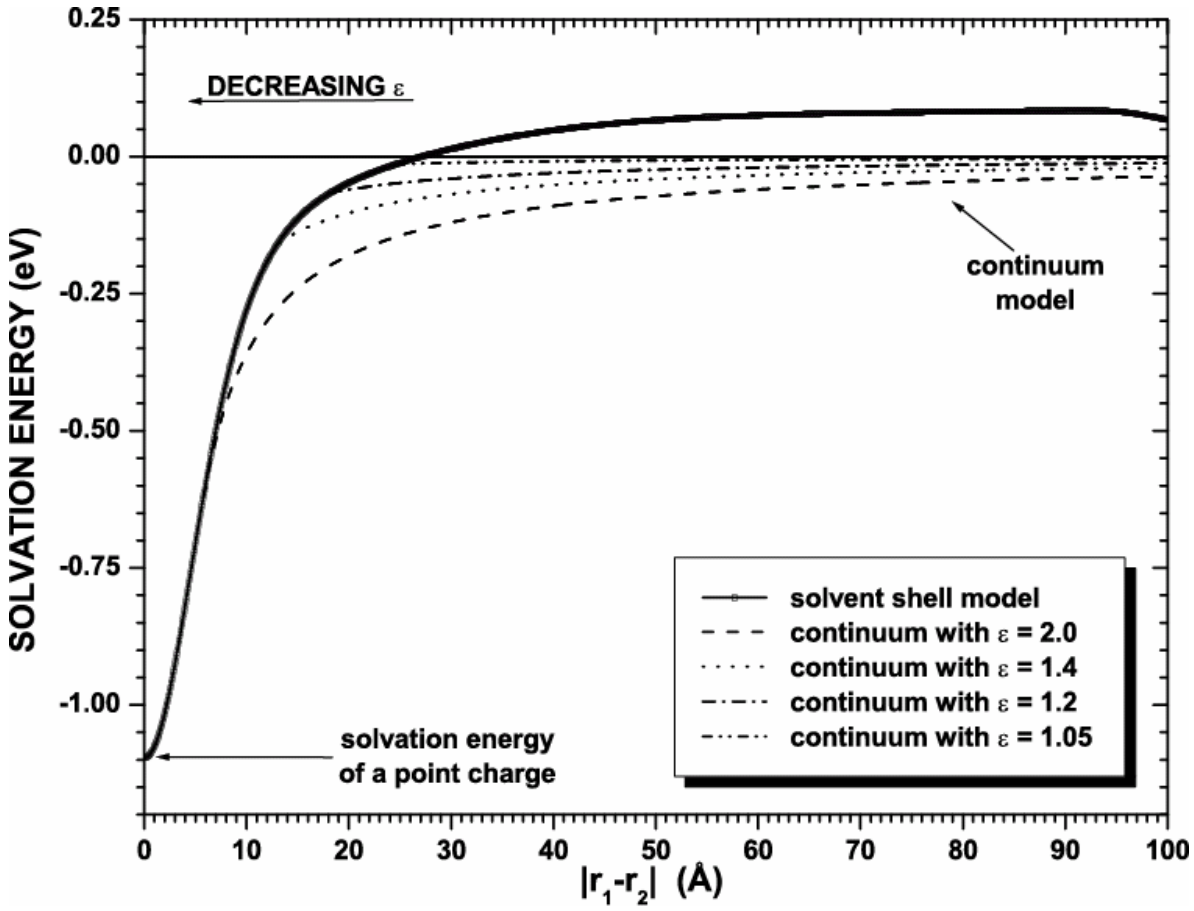

Fig. S3. The dielectric screening function $G\left(\left|\mathbf{r}_i - \mathbf{r}_j\right|\right)$. The solid line is from explicit calculations on charges placed in a cylinder of polyacetylene. The effects due to the finite size of the cylinder are removed by splicing with the long range form appropriate for a continuous dielectric with a dielectric constant of 2.0.

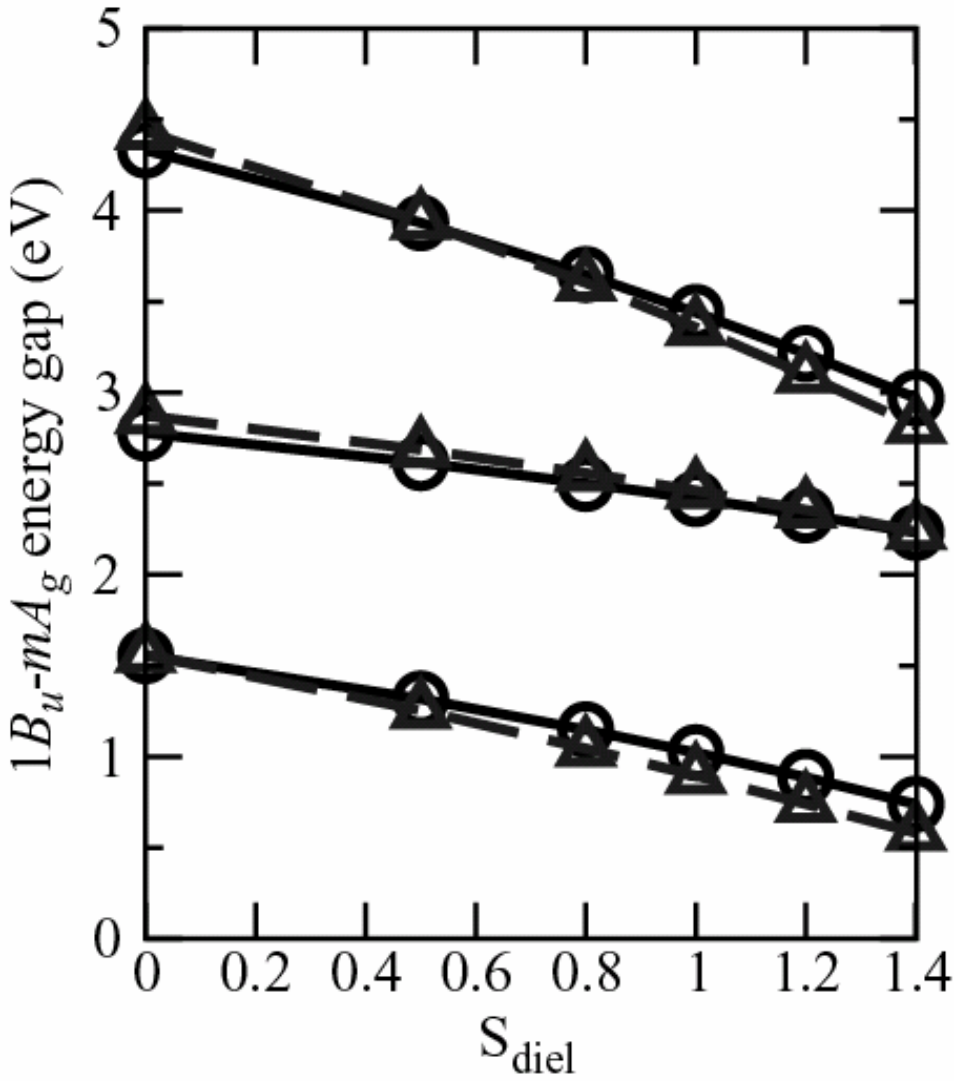

Fig. S4. The effect of dielectric screening on the excited state energies for PPV-8 and OPPV-9. Energies of the mA_g, $1B_u$ states, and the $1B_u$-mA_g energy gap are plotted from top to bottom. The X-axis is the solvation scaling factor which is proportional to the dielectric constant of the medium. Full SCI is performed. The circles stand for OPPV-9, and the triangles represent PPV-8.

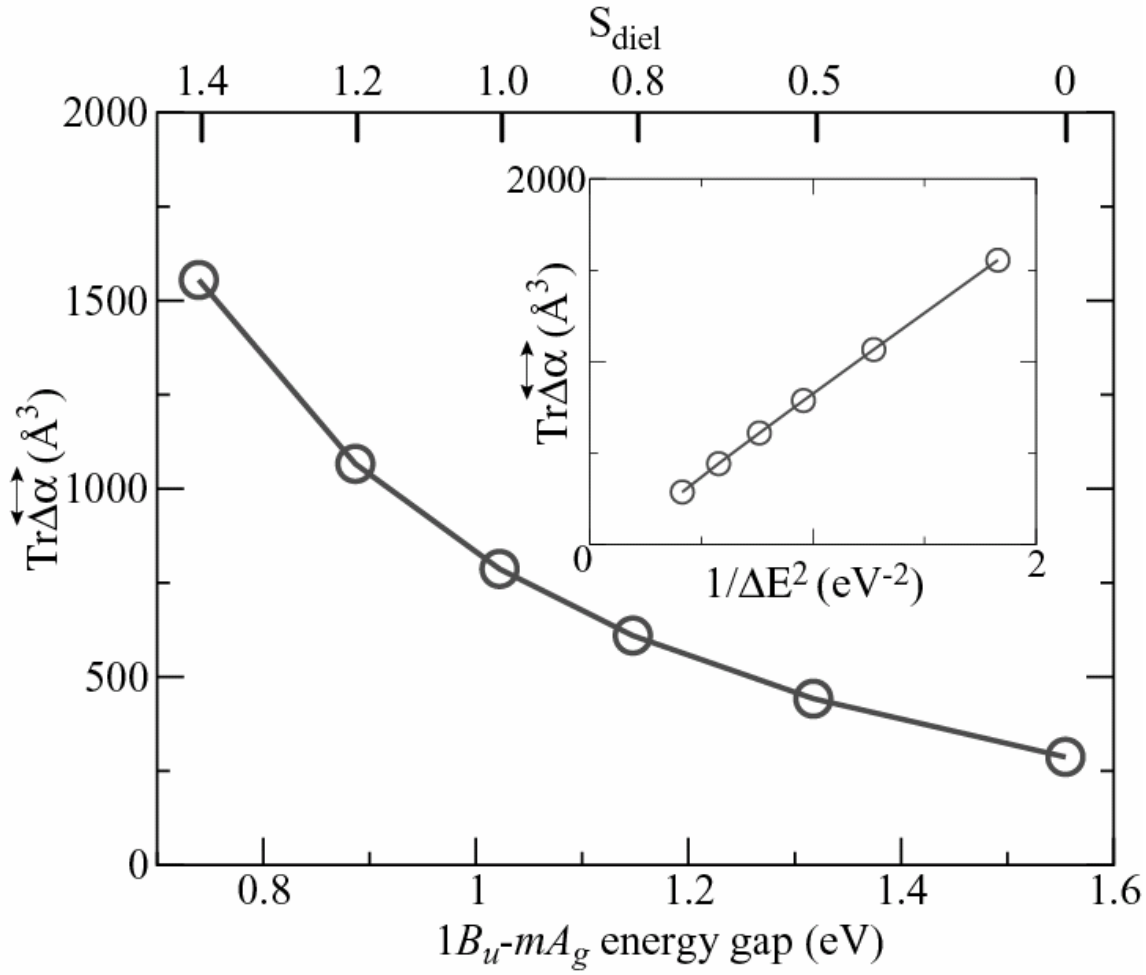

Fig. S5. The effect of dielectric solvation on the polarizability change for OPPV-9. The upper X-axis is the solvation scaling factor (the same as in Fig. S4). The lower X-axis is the energy separation between mA_g and $1B_u$ states, and the Y-axis is the polarizability change from the ground state to the $1B_u$ state, $Tr\overleftrightarrow{\Delta\alpha}$. The inset shows the linear relationship between these two properties. Full SCI is performed.